

# Appendix C

## Calibration Data

### C.1 Gas Pulse Width

The duration of the target gas pulse was determined by measuring the elastic electron scattering signal in the collision chamber (see Section 2.3), while pulsing a test gas such as He. In these experiments the elastic counts were accumulated over a number of  $250 \mu\text{s}$  windows, and the count window was then delayed at increasing time intervals with respect to the pulser fire command from the timing box. A typical result from such an experiment is shown in Figure C.1.1. In this particular experiment gas was introduced into the apparatus at 800 mbar and elastic counts from a 50 eV incident beam were detected in the  $75^\circ$  RFA detector. The full-width-at-half-maximum (FWHM) of the gas pulse in Figure C.1.1 is about 1.5 ms, which is significantly longer than the  $200 \mu\text{s}$  duration of the pulsed nozzle driver's electrical pulse. The gas pulses are of this duration for all the experiments reported earlier in this thesis.

### C.2 Electron Scattering Energy Resolution

The combined energy resolution of the monochromator/RFA was measured by accumulating elastically scattered electron counts in one of the detectors as the potential on  $RFA_2$  was varied (Figure C.2.1), while pulsing He gas through the system.

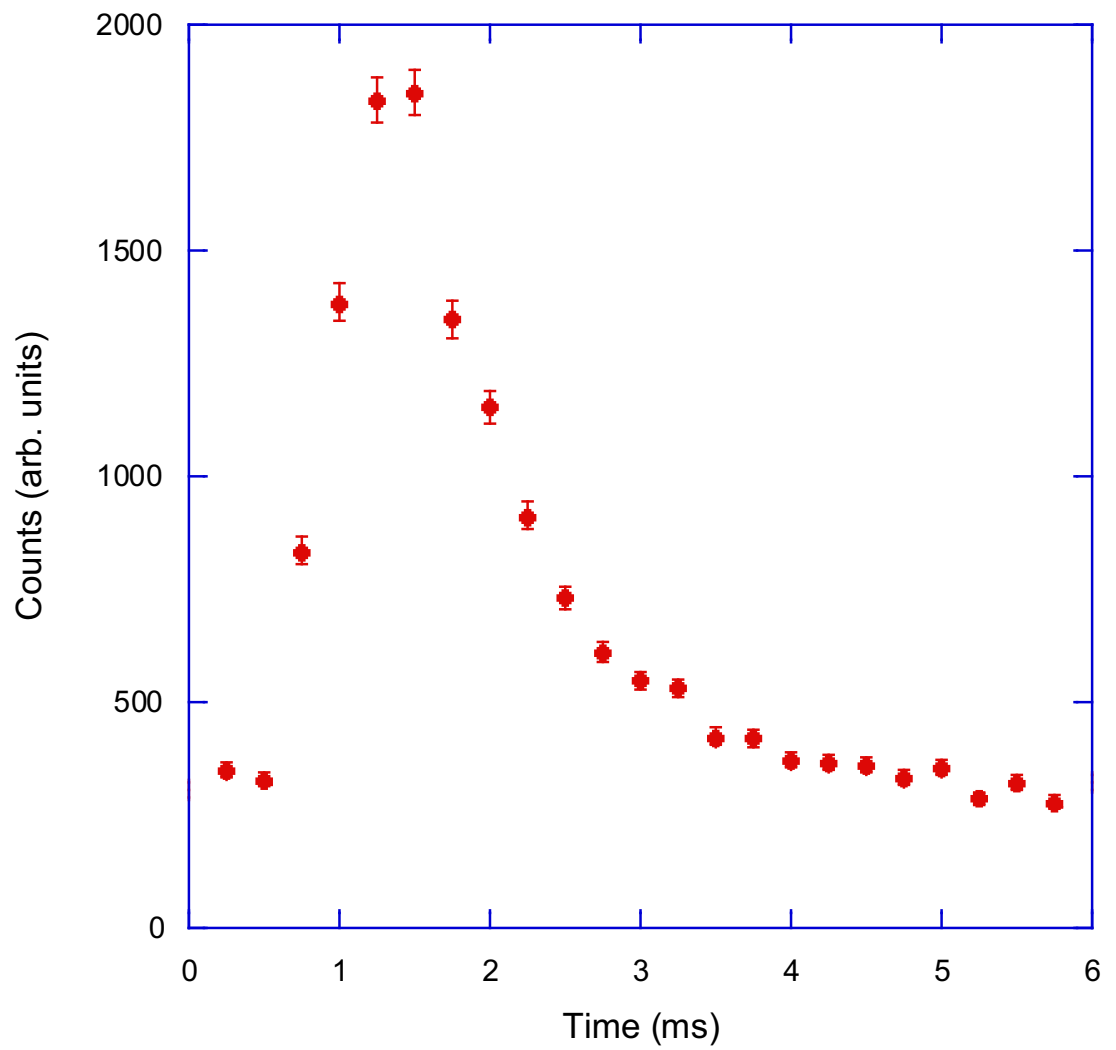


Figure C.1.1: Scattered electron counts ( $\bullet$ ) as a function of time from the pulser fire command. The error bars represent the statistical variation in the counts.

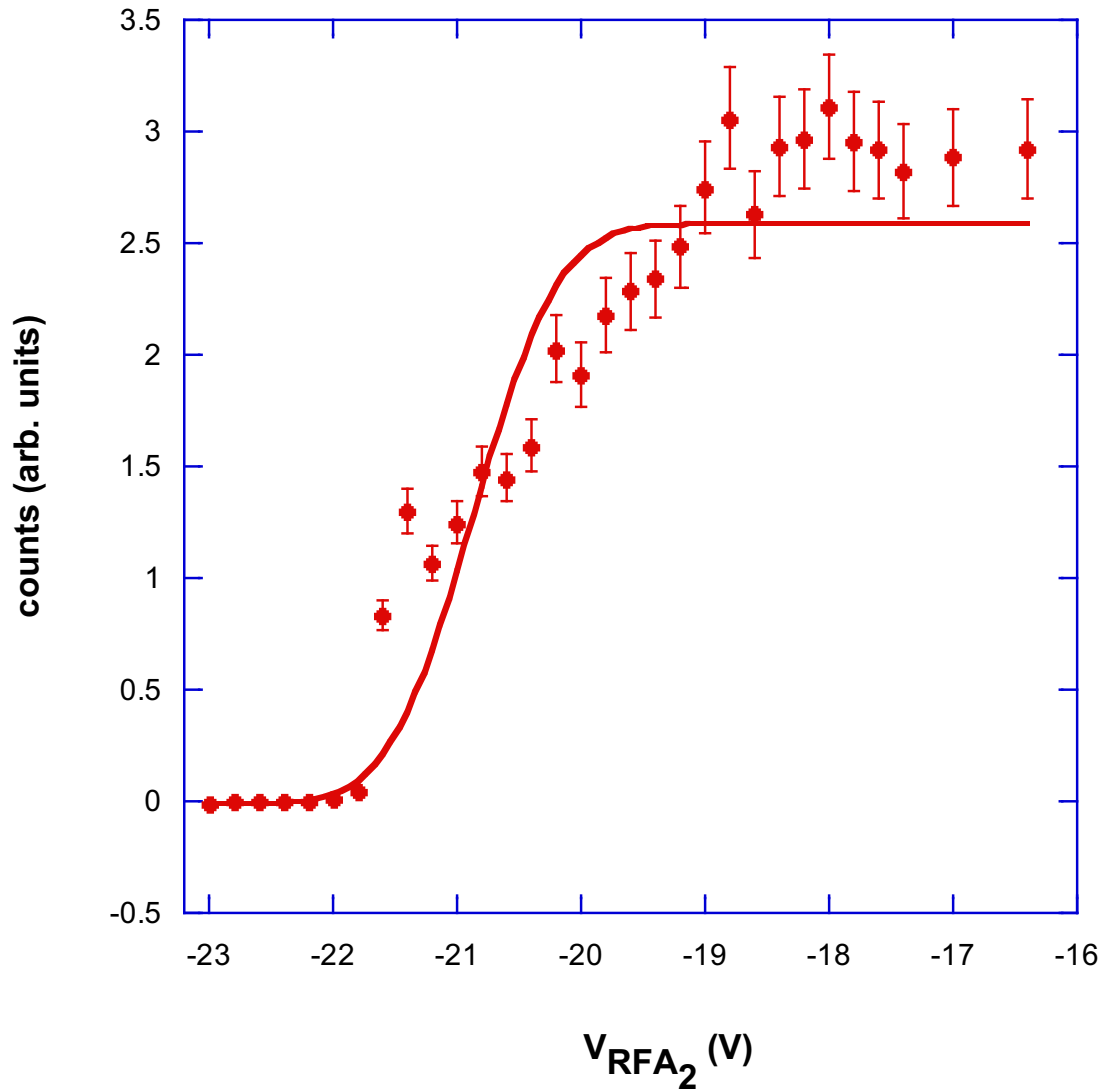


Figure C.2.1: A typical result ( $\bullet$ ) for our experiments to determine the energy resolution of the system. The incident electron beam is nominally at 22 eV incident energy, with scattered electrons being detected in the  $90^\circ$  RFA detector. The solid curve represents a fit to the data (equation (C.2.1)). The error bars indicate the variations in the scattered counts due to both statistical variations and pulse-by-pulse gas density variations.

An integrated Gaussian function was then fitted to the scattering data, ie.:

$$\dot{N}^e(V_{RFA_2}) = A \int_{-\infty}^{V_{RFA_2}} \exp\left(-\left(\frac{V - V_c}{\sigma}\right)^2\right) dV, \quad (\text{C.2.1})$$

where  $A$  is the Gaussian amplitude,  $V_c$  is the Gaussian centre position and  $\sigma$  is the Gaussian width. The FWHM system resolution was then determined from the  $\sigma$  parameter. In the example shown in Figure C.2.1, the energy resolution is 1.30 eV for a 20 eV beam ( $\Delta E_A/E_A=0.065$ ), which is similar to the theoretical optimal energy resolution ( $\Delta E_A/E_A=0.061$ ) calculated in Section 2.3.2.

It is also apparent from Figure C.2.1 that the energy profile shows deviations from the pure Gaussian profile. The slope of the data is underestimated by the fit function near cutoff, overestimated near saturation, and the saturation value itself is underestimated. The  $\chi^2_\nu$  for this functional form is 32, indicating that there is essentially zero chance that the observed deviation from the fit function is due to random variations. To investigate this discrepancy the RFAs were modelled using commercial software (Simion 6.0). The experiment was simulated using the Simion model and a similar deviation from a Gaussian profile was observed. The observed performance of the RFAs is therefore some feature inherent to their design, either due to electrons being lensed by the RFA apertures, or perturbations in the electric field by the analyser wall and ceramic spacers. However, in spite of the deviations from the fit function, an integrated Gaussian function still served as a useful model to estimate the system's overall energy resolution.

### C.3 TOFMS Characterisations

The TOFMS was optimised by monitoring the ion signal from chlorobenzene ( $\text{C}_6\text{H}_5\text{Cl}$ ), as the experimental conditions were varied. The first ionisation threshold of chlorobenzene is 9.08 eV [97], which is well below the 10.48 eV ionisation limit of the TOFMS.

## TOFMS Resolution

The second order space focusing of the TOFMS was optimised by setting the repeller at a constant potential (3000 V), while ramping the extractor potential and monitoring the width of the  $C_6H_5Cl$  ion spike in the final TOF spectra (Figure C.3.1), which was averaged over 1000 laser shots.

To determine the location of the minimum in Figure C.3.1, a second-order polynomial was fitted to the data. The minimum was then calculated from the fit parameters, yielding a value of  $V_{Ex}=1772\pm 92$  V. The uncertainty limit is calculated here as the quadrature sum of the uncertainties in the fit parameters. According to the space focusing equations the optimal potential with  $V_{Rp}=3000$  V is  $V_{Ex}=1885$  V, which is only marginally outside the uncertainty limit of the observed minimum. This small discrepancy is probably due to non-uniformities in the electric field, due to the pathways cut in the rings to allow the passage of the target beam and the laser. The acceleration of extracted ions between the grounded end of the flight tube and the field suppression grid may also have contributed to this small discrepancy.

The present TOFMS was designed to resolve one proton mass differences over a range of masses. Figure C.3.2 shows a 1000 waveform averaged TOF spectrum, for a target beam containing a mixture of three halogenated benzene molecules ( $C_6H_5F$ ,  $C_6H_5Cl$ ,  $C_6H_4F_2$ ). Here, the separation of the  $C_6H_5Cl$  and  $C_6H_4F_2$  ion spikes (112.5 and 114 amu, respectively) is highlighted.

The resolution ( $R$ ) of the mass spectrometer, at a mass  $M$ , is defined as [52]:

$$R = \frac{M\Delta t_{\Delta M=1}}{\Delta t_{FWHM}}, \quad (C.3.1)$$

where  $\Delta t_{\Delta M=1}$  is the time difference between adjacent masses and  $\Delta t_{FWHM}$  is the FWHM spread in arrival times of ions at a particular mass. The mass resolution of the present TOFMS is  $R=216$  at mass 114 (Figure C.3.2). This mass resolution improves at lower masses, as demonstrated in the TOF spectrum for

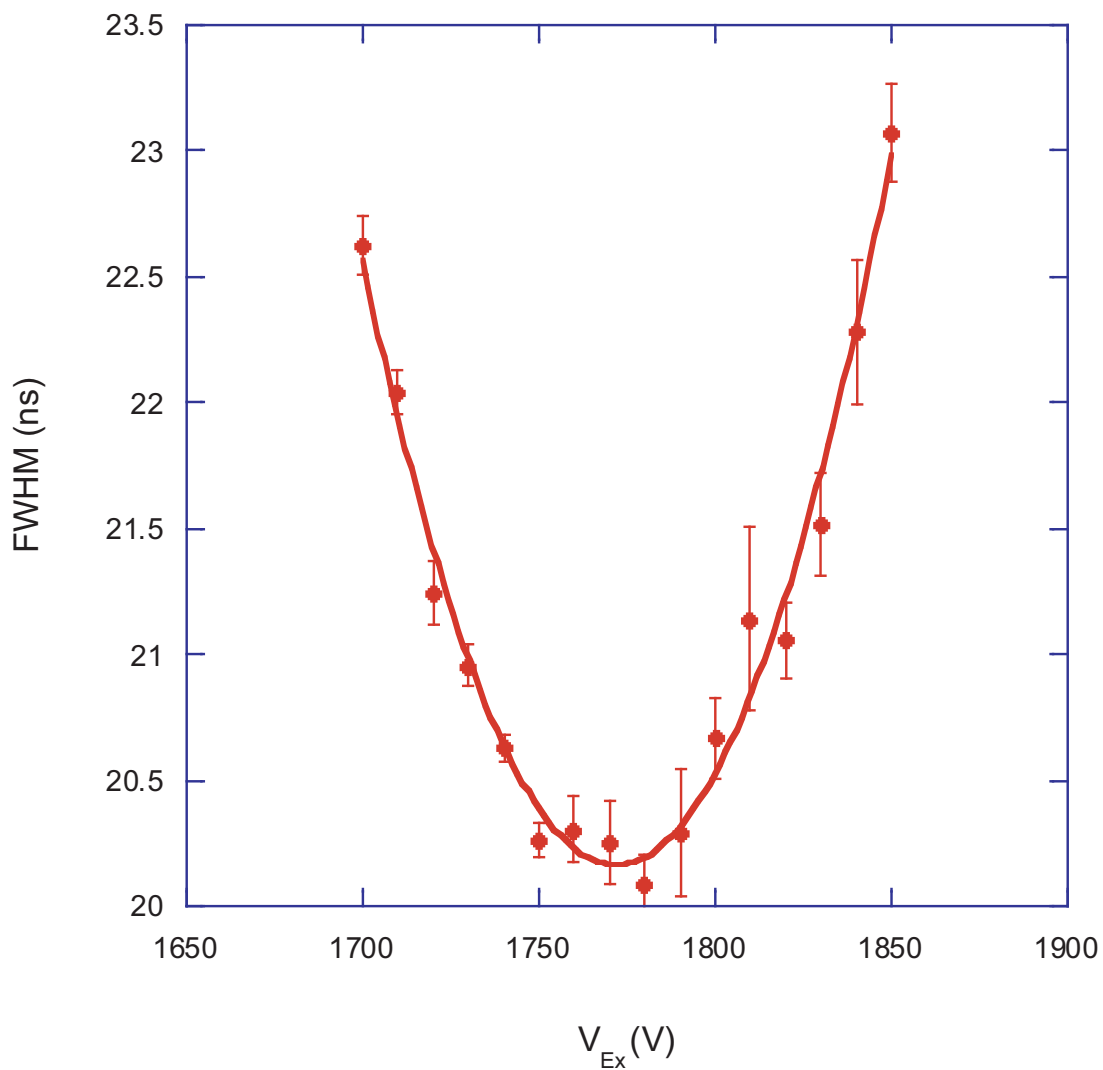


Figure C.3.1: FWHM of the  $\text{C}_6\text{H}_5\text{Cl}$  ion signal ( $\bullet$ ) as a function of the extractor potential. A second-order polynomial model function (full curve) has been fitted to this data. The error bars represent the statistical variation in the ion signal.

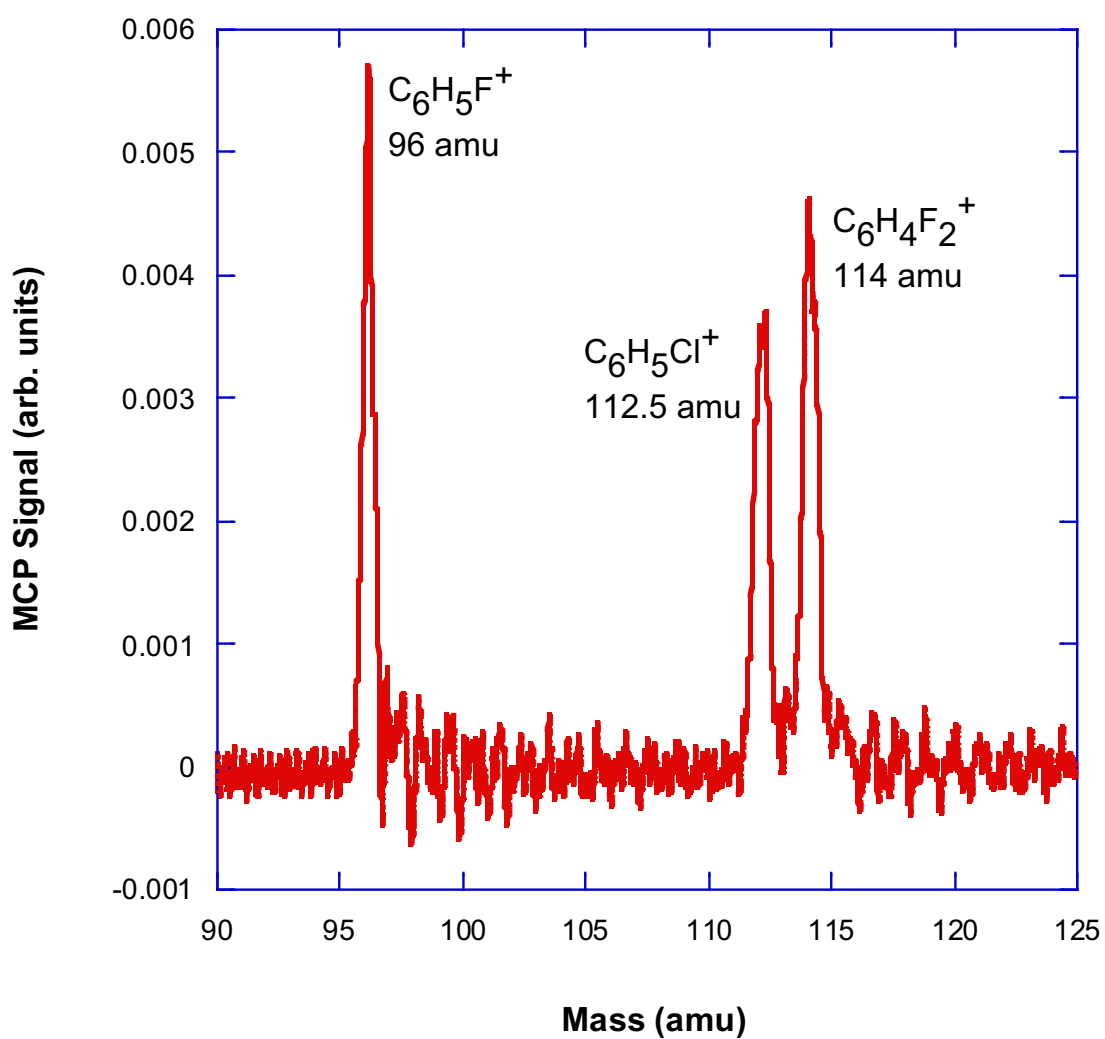


Figure C.3.2: A typical TOF spectrum for a series of halogenated benzenes.

the photofragments of allene (Figure A.2.1), where the mass resolution is now  $R=349$  at mass 40.

## 118nm VUV Optimisation

The optimal conditions for 118 nm VUV generation, using pure Xe as the tripling medium, were determined by monitoring the intensity of the  $C_6H_5Cl$  ion peak, over 1000 laser shots, as the Xe pressure was varied (Figure C.3.3).

To identify the peak Xe pressure, a model function of the form described in Björklund [98] was fitted to the Xe data (Figure C.3.3). The peak ion intensity was then calculated from the fit parameters, yielding an optimal Xe pressure of  $7.0\pm 0.2$  Torr. The uncertainty limit was calculated as the quadrature sum of the uncertainties on the fit parameters.

To specify the optimal conditions for 118 nm VUV generation when a Xe and Ar gas mixture was used as the tripling medium, Xe was added to the gas cell at a fixed gas pressure and the intensity of chlorobenzene ions in the TOFMS was monitored as Ar was then added to the cell. The result of such an experiment, for partial Xe pressures of 5 Torr and 10 Torr, is shown in Figure C.3.4.

The Xe+Ar data indicates that, for both gas mixtures, the optimum ratio of Xe:Ar was approximately 1:11. Experiments were also conducted at higher partial Xe pressures, however, the signal in the detector peaked at the same level as in the 10 Torr measurement. Since the 118 nm intensity should increase as the square of the Xe pressure [98], the ion signal was concluded to be saturating the MCP detector. While the 355 nm power could have been further reduced so that the ion signal would not saturate, and the experiment then repeated, the photoionisation source was concluded to produce ample 118 nm VUV and so no further investigation of the optimal 118 nm production conditions were conducted. For most of the TOF experiments reported in this thesis, the pressure of Xe in

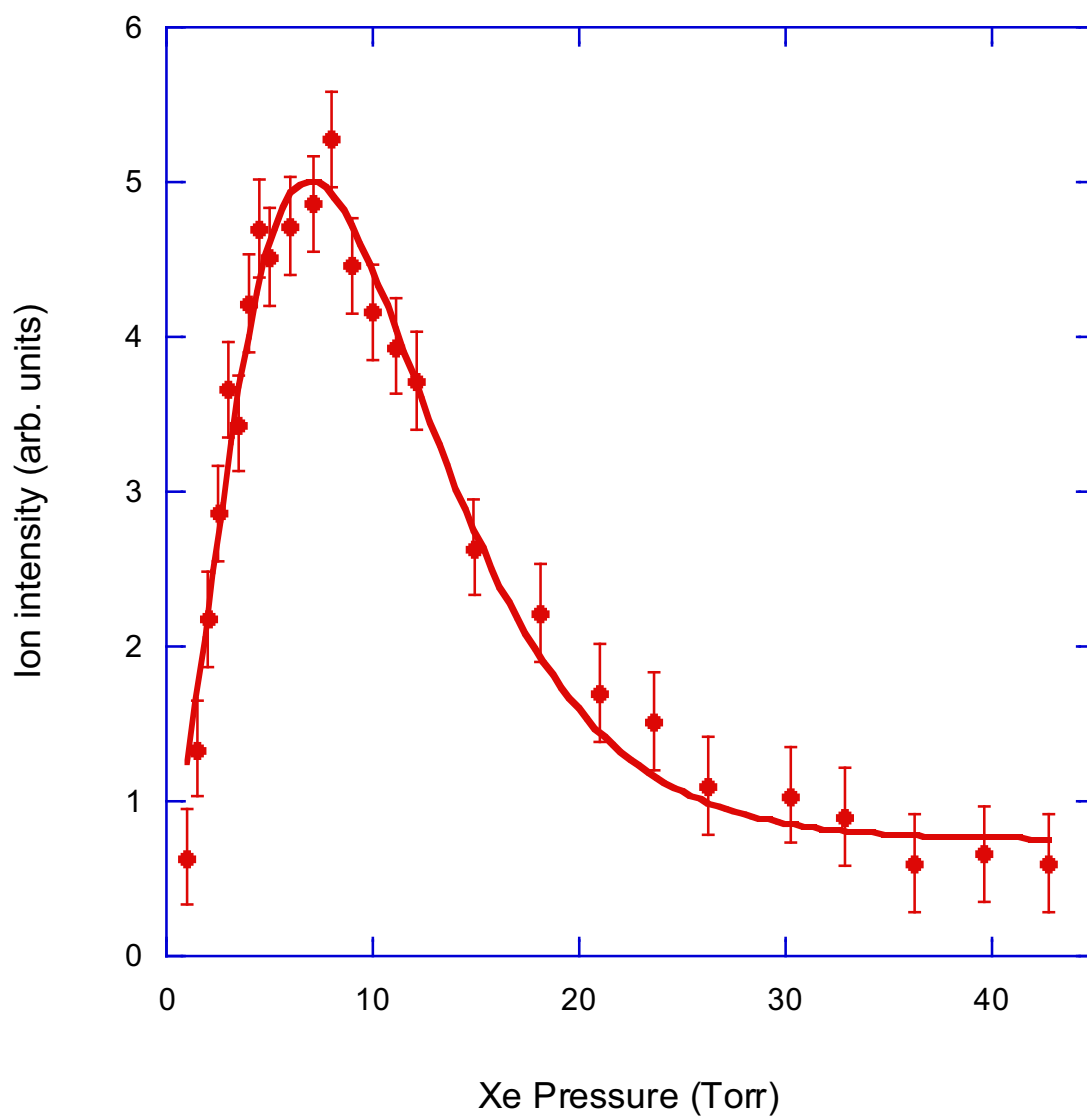


Figure C.3.3:  $\text{C}_6\text{H}_5\text{Cl}$  ion intensity ( $\bullet$ ) as a function of the Xe pressure in the frequency tripling cell. The error bars represent the statistical variation in the  $\text{C}_6\text{H}_5\text{Cl}$  ion signal.

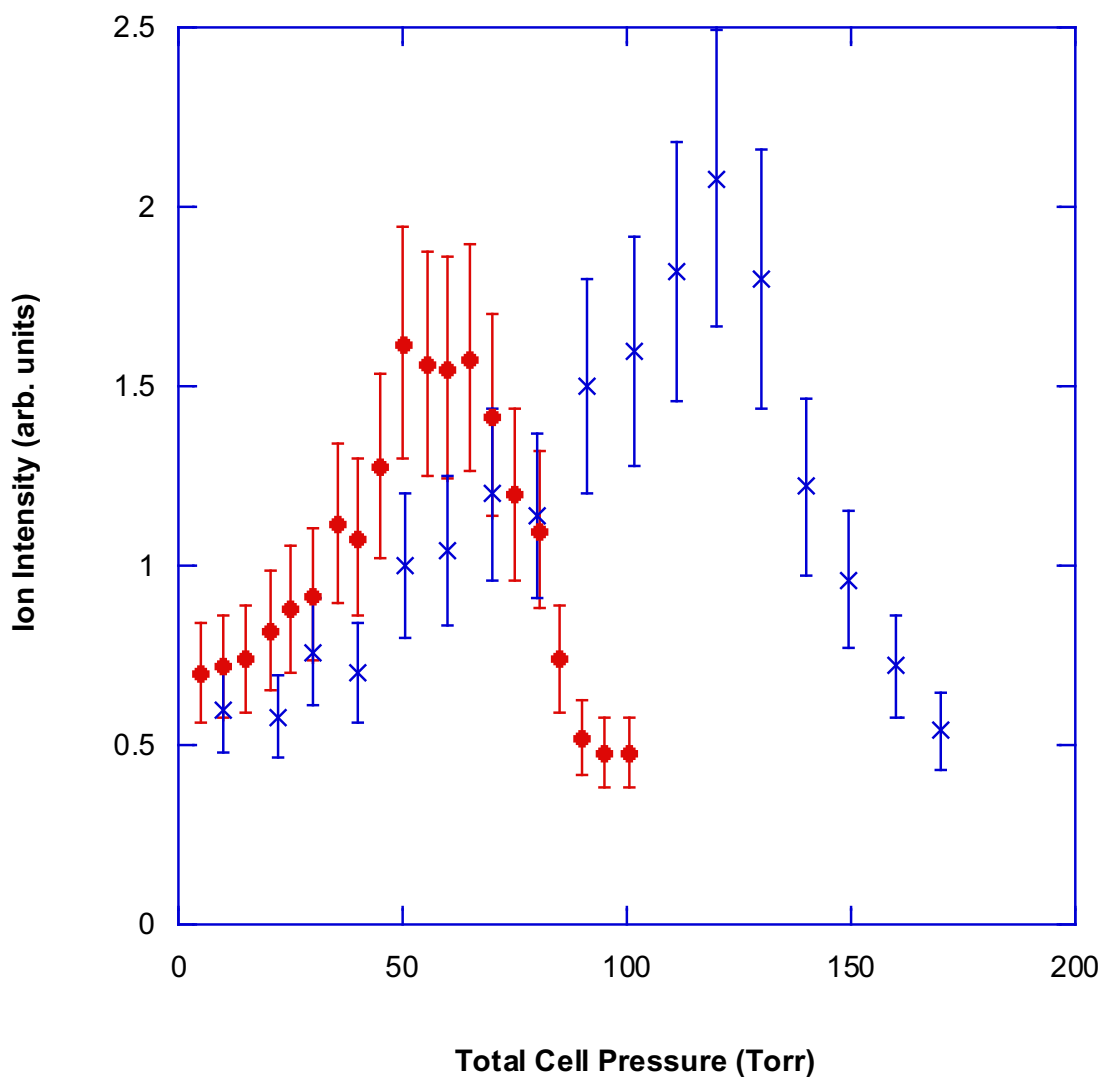


Figure C.3.4: Intensity of  $C_6H_5Cl$  ions detected in the TOFMS as a function of the pressure in the frequency tripling cell when a Xe/Ar mixture was used as the tripling medium. Results are shown for partial Xe pressures of 5 Torr ( $\bullet$ ) and 10 Torr ( $\times$ ). The error bars represent the statistical variation in the  $C_6H_5Cl$  ion signal. A fit function (solid curve), of the form described in Björklund [98], has been fitted to the data.

the cell was kept below 5 Torr and, whatever value was used, Ar added at a 1:11 ratio.